remote sensing

MDPI

Article

Infrared Dim Star Background Suppression Method Based on Recursive Moving Target Indication

Lei Zhang [1], Peng Rao [2,3,*], Yang Hong [2,3,4], Xin Chen [2,3] and Liangjie Jia [2,3,4]

[1] College of Astronautics, Nanjing University of Aeronautics and Astronautics, Nanjing 210016, China
[2] Shanghai Institute of Technical Physics, Chinese Academy of Sciences, Shanghai 200083, China; hongyang@mail.sitp.ac.cn (Y.H.); chenxin@mail.sitp.ac.cn (X.C.); jialiangjie@mail.sitp.ac.cn (L.J.)
[3] Key Laboratory of Intelligent Infrared Perception, Chinese Academy of Sciences, Shanghai 200083, China
[4] University of Chinese Academy of Sciences, Beijing 100049, China
* Correspondence: peng_rao@mail.sitp.ac.cn

Abstract: Space-based infrared target detection can provide full-time and full-weather observation of targets, thus it is of significance in space security. However, the presence of stars in the background can severely affect the accuracy and real-time performance of infrared dim and small target detection, making star suppression a key technology and hot spot in the field of space target detection. The existing star suppression algorithms are all oriented towards the detection before track method and rely on the single image properties of the stars. They can only effectively suppress bright stars with a high signal-to-noise ratio (SNR). To address this problem, we propose a new method for infrared dim star background suppression based on recursive moving target indication (RMTI). Our proposed method is based on a more direct analysis of the image sequence itself, which will lead to more robust and accurate background suppression. The method first obtains the motion information of stars through satellite motion or key star registration. Then, the advanced RMTI algorithm is used to enhance the stars in the image. Finally, the mask of suppressing stars is generated by an accumulation frame adaptive threshold. The experimental results show that the algorithm has a less than 8.73% leakage suppression rate for stars with an SNR ≤ 2 and a false suppression rate of less than 2.3%. The validity of the proposed method is verified in real data. Compared with the existing methods, the method proposed in this paper can stably suppress stars with a lower SNR.

Keywords: star background suppression; recursive moving target indication; dim space target detection

Citation: Zhang, L.; Rao, P.; Hong, Y.; Chen, X.; Jia, L. Infrared Dim Star Background Suppression Method Based on Recursive Moving Target Indication. *Remote Sens.* **2023**, *15*, 4152. https://doi.org/10.3390/rs15174152

Academic Editor: Paolo Tripicchio

Received: 24 July 2023
Revised: 21 August 2023
Accepted: 23 August 2023
Published: 24 August 2023

1. Introduction

The utilization of space resources has led to an increase in space debris, asteroids, and failed satellites, which pose a serious threat to working satellites [1,2]. Ensuring space security is a vital mission, and the ability to surveil these space targets is essential in achieving this goal [3,4]. Space infrared remote sensing provides full-time and full-weather observation of objects, making it the main tool for surveilling space targets. However, due to the long detection range, limited resolution, low radiant energy, and small target size, these space targets appear as dim point targets in the focal plane [5–9]. These low signal-to-noise ratio (SNR) point targets are inherently difficult to detect, especially with complex backgrounds and noise [10–14]. Therefore, background suppression is crucial for space target observation.

Stars are a crucial component of the deep space background and, like other space targets, appear as point sources in images [15,16]. However, stars are a significant source of false alarms in space target detection [17,18]. If the star background cannot be effectively suppressed, it can negatively impact the accuracy and real-time performance of the detection process [19,20]. While most algorithms proposed in the past few decades have focused on clearing bright stars as part of high-SNR target detection, few have addressed

the suppression of dim stars. A few algorithms that can suppress dim stars are limited by specific application conditions. Nevertheless, the presence of dim stars in the background cannot be ignored. Therefore, this paper aims to propose a universal dim star background suppression method that can ensure the accurate and real-time detection of low-SNR targets.

1.1. Research Status

Detecting stars in space images can be challenging due to their similar characteristics to other space targets. Existing algorithms can be generally classified into two kinds, which are based on star catalogue and image. The algorithms based on images often rely on multi-frame images to introduce kinematic characteristics. Stars, being stationary in celestial coordinates for short periods, can be distinguished from other moving space targets [21]. Spatial–temporal correlation information is used to classify detection methods into two categories: space before time (SBT) and time before space (TBS). Previous research has explored both approaches. SBT methods prioritize spatial information before temporal [22–26], while TBS methods prioritize temporal information before spatial [27–31].

SBT utilizes the detection before track (DBT) method to detect potential targets, which may include stars. Then, stars are stationary in celestial coordinates and have fixed positions relative to each other in time, while real space targets and stars constantly change positions, as shown in Figure 1. The blue stars present stars and the red point presents space targets. Therefore, SBT can suppress stars from other space targets by extracting the position information of potential targets from a single frame. This approach allows for more accurate tracking of real space targets.

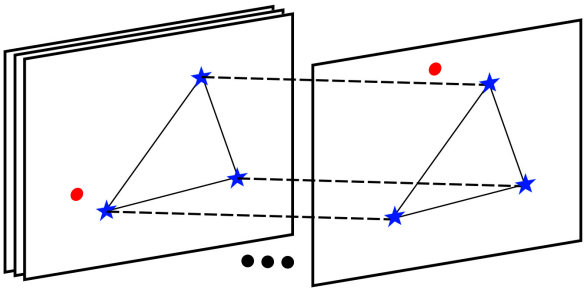

Figure 1. The schematic of stars suppression of SBT.

For instance, Hong Zhang et al. [22] define a feature space of distance (FSD) between stars to describe the invariance of distance among the stars. This method is used for feature matching and image transformation to achieve image registration. After image registration, the star background can be easily suppressed by the image difference. Other SBT methods based on star image registration adopt different matching features and registration algorithms. Yu Zhu et al. [23] propose the longest common sub-sequence (LCS) to find the isomorphism sub-graph which represents the matched feature pairs. Qingqing Luo et al. [24] introduce an iterative closest point algorithm which is a widely used point cloud registration algorithm. They also proposed a Gaussian mixture probability hypothesis density filter to avoid the target being mistakenly associated with stars. Feng Liu et al. [25] apply a mature and effective triangle algorithm to register stars. Meanwhile, target motion track detection is also considered to further suppress noise. Recently, the interior angle matrix has been used to describe the topological invariance of stars [26]. Then, stars are suppressed by sequence frame offset statistics histogram.

SBT methods rely on detecting stars using a single frame, which severely limits the SNR of suppressed stars. As a result, these methods are not suitable for aiding the detection of very-low-SNR targets.

Figure 2 illustrates the TBS method, which utilizes the position invariant theory to identify potential targets. The blue stars present stars and the red point presents space

targets. The black line denotes the movement of the target and the star. Unlike SBT, TBS accumulates the energy of potential targets from the time dimension. This allows all potential targets to gain their corresponding route. The route of space targets is markedly different from the route of stars, whether the field of the camera is moving or still. By identifying the routes of space targets, TBS can suppress the stars and effectively identify potential targets.

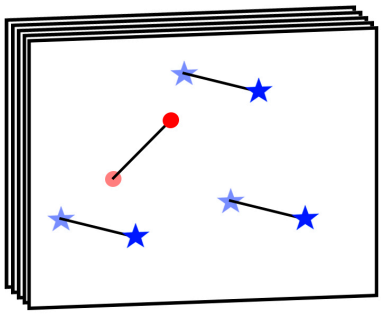

Figure 2. The schematic of stars suppression of SBT.

The key to TBS is to identify the route difference to suppress stars. Wang Hou et al. [27] propose a main directional suppression high pass filter for star line suppression, which considers the phase of the spectrum as the velocity of the target. Similarly, an adaptive linear filtering method is proposed to decrease the influence region of stars filtering uniformly [28]. Furthermore, the moving target indicator (MTI) algorithm is an effective trajectory detection method that achieves target detection and star suppression through route energy accumulation and direction judgment [29]. Another set of TBS methods focuses on the still field of the camera. Interval frame subtraction is applied to suppress stars, and back neighborhood frame correlation is proposed to protect the targets covered by stars [30]. Additionally, a star subtraction mask is obtained by introducing the maximum frame and medium frame, which can suppress the still star residues [31].

The preceding methods are highly dependent on their corresponding target detection methods, making them challenging to apply to alternative methods. Furthermore, the use of multiple frames superimposition is utilized to derive the star route, but this approach has limited energy enhancement and is unable to effectively suppress stars with a very low SNR.

The algorithms based on star catalogue are theoretically not limited by the SNR of stars. According to the reference method of the star catalogue, it can be divided into two categories. The first is star identification. Star identification determines the correspondence between stars based on the feature matching of the star catalogue consisting of the observed stars in the field of view. Star identification is the key technic of satellite position confirmation from the star sensor. To pursue a faster and more robust star identification performance, neural networks [32], color ratio information [33], rotation-invariant additive vector sequence [34], and so on are introduced and have obtained good results. In the application of star suppression, star identification matches the stars in the image for suppression. These algorithms can suppress all the stars recorded by the star catalogue regardless of the SNR. The second is the star map mask. These algorithms generate a star mask from the observation direction and star catalogue [35]. Like star identification, these algorithms are not limited by star SNR because they rely on star catalogue.

In addition to the previously mentioned methods, there exist various algorithms for star observation. Some of these algorithms aim to suppress stars or enhance them. For example, one approach involves using two spectral band sensors to estimate the temperature of targets and differentiate stars based on temperature differences [19]. However, this method requires high-quality detection hardware. In cases where the target is at a finite distance and its scale is larger than 3×3 pixels [36], connected components analysis can be used to cluster stars. This method cannot be generalized to other applications.

Currently, neural networks are widely used for the classification of remote sensing image data. An improved CBDNet network structure has been proposed for star background suppression, which is trained using real images [37]. However, it is important to note that the signal-to-noise ratio (SNR) of stars that this algorithm can handle is limited.

In conclusion, there is no universal infrared dim star background suppression. The algorithms based on images are mainly used to suppress the high-SNR star background. Although the algorithms based on star catalogue can suppress low-SNR stars, it is not suitable for the preprocessing of space target detection and tracking. These algorithms may suppress some stars that are not in the image, causing information loss and consuming more computing resources. Other algorithms require specific application conditions that are not universally applicable. If the large amounts of dim infrared stars cannot be suppressed by preprocessing, the real-time on-board intelligent information processing would be catastrophic. Therefore, an effective and less consuming infrared dim star background suppression method is vitally important in practical application.

1.2. Motivation

Previous research has largely overlooked the impact of very-low-SNR stars that cannot be detected using a single frame. While these stars may not significantly affect the performance of DBT methods, they can still hurt real-time performance and accuracy in TBD methods. Existing TBD methods, such as particle filter [38,39], dynamic programming [40,41], and Hough transform [42,43], have primarily focused on digging targets that are covered by heavy noise. Usually, these TBD methods need extra processes to identify real targets and stars, which can negatively impact real-time performance and accuracy. For instance, the particle filter may cancel the route of stars, but the small number of stars as potential targets requires a large number of additional particles to track, which can waste computing resources and negatively affect real-time performance.

The main contributions of this paper are as follows: (1) Recursive moving target indication (RMTI) is improved in a motion vector to enhance dim stars efficiently and accurately. (2) An adaptive multi-frame accumulation threshold segmentation is proposed, which can create an accurate star mask. Dim stars can be suppressed in real-time. (3) The set value of key parameters is provided by analyzing the experiment. Meanwhile, a simulation experiment was designed to verify the feasibility and robustness of this method. The proposed algorithm fills the low-SNR star background suppression gap in space target detection and tracking. It can be used as an efficient preprocessing step for most target detection and tracking methods and has great practical value.

The remainder of this paper is structured as follows. Section 2 provides a detailed explanation of our method. In Section 3, we present our experimental approach, including the set values of main parameters and the resulting experimental results. Section 4 discusses the performance of our proposed methods. Finally, in Section 5, we present our conclusions.

2. Methodology

Figure 3 displays the block diagram of the proposed infrared dim star background suppression method based on recursive moving target indication. Firstly, the star motion is extracted from the high-SNR star map or is deduced from the satellite attitude and orbit data. Then, the RMTI is used to enhance the dim star and generate the frame mask of multi-frame accumulation (FMMA). The FMMA carries the number of frames that have been accumulated for each pixel. Therefore, the adaptive threshold for each pixel is derived by FMMA. Finally, the star mask can be extracted from a multi-frame enhanced star image using adaptive threshold segmentation. The dim stars can be suppressed by the star mask.

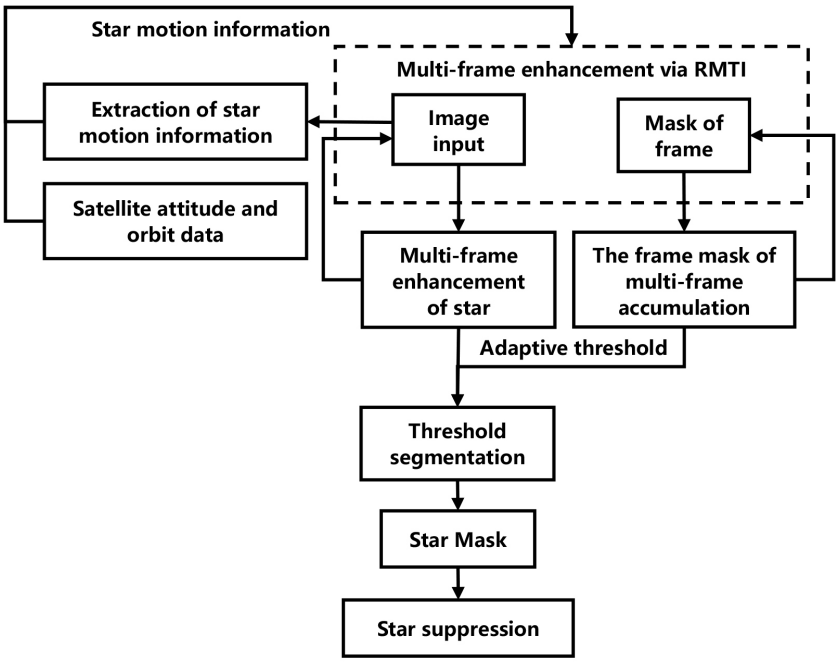

Figure 3. Block diagram of the proposed infrared dim star background suppression method.

2.1. The Multi-Frame Enhancement of Advanced RMTI

RMTI can produce significant SNR gains when the target motion state is known [44,45]. Unlike noncooperative targets, such as space debris, stars remain stationary relative to the Earth. As a result, estimating the motion information of stars in an image sequence is a relatively simple task. The phase matrix of the motion spectrum for each frame can be calculated based on the star motion information, and the spectrum of the current enhanced frame can be obtained by multiplying the phase matrix of the motion spectrum for the current frame and the spectrum of the previous enhanced frames. In the space domain, RMTI enhances stars by registration and accumulation [46]. RMTI processes each frame and stores the result for further processing. The output of the previous frame is used as the input for the next frame, allowing for easy adaptation to digital processing.

To continuously, accurately, and efficiently enhance the star, we improve the RMTI in the motion vector. The multi-frame enhancement of RMTI for stars proceeds is described below. The signal intensity of the star in the focal plane is denoted by $s(\boldsymbol{r}, nt_0)$, where $\boldsymbol{r}$ represents the coordinate of stars, and t_0 is the image sampling period. The star state transition function is defined as

$$s(\boldsymbol{r}, nt_0) = s(\boldsymbol{r} - \boldsymbol{v_n} t_0, (n-1)t_0) \tag{1}$$

where $\boldsymbol{v_n}$ is the velocity of the stars in nt_0. The image $y(\boldsymbol{r}, nt_0)$ can be described as:

$$y(\boldsymbol{r}, nt_0) = s(\boldsymbol{r}, nt_0) + n(\boldsymbol{r}, nt_0) \tag{2}$$

where $n(\boldsymbol{r}, nt_0)$ represents the noise of the image. The two-dimensional spatial Fourier transform of the image is:

$$Y(\boldsymbol{k}, nt_0) = S_{n-1}(\boldsymbol{k}) exp\{-i\boldsymbol{k} \cdot \boldsymbol{v_n} t_0\} + N(\boldsymbol{k}, nt_0) \tag{3}$$

where $\boldsymbol{k}$ denotes a two-dimensional spatial wavenumber vector. $S_{n-1}(\boldsymbol{k})$ denotes the two-dimensional spatial Fourier transform of the star signal of the previous frame, and $N(\boldsymbol{k}, nt_0)$ is the two-dimensional spatial Fourier transform of noise. The star registration of adjacent frames in the space domain can be achieved by multiplying $exp\{-i\boldsymbol{k} \cdot \boldsymbol{v_n} t_0\}$ in the frequency domain. For convenience, let $\alpha_n = exp\{-i\boldsymbol{k} \cdot \boldsymbol{v_n} t_0\}$. α_n is the phase matrix of the

motion spectrum for nt_0. When $n = 0$, the two-dimensional spatial Fourier transform of the image is:

$$Y(\boldsymbol{k}, 0) = S_0(\boldsymbol{k}) + N(\boldsymbol{k}, 0) \tag{4}$$

Let $X_0(k) = Y(\boldsymbol{k}, 0)$, where $X_n(k)$ denotes the enhanced frequency spectrum of stars. When $n = 1$, the two-dimensional spatial Fourier transform of the image is:

$$Y(\boldsymbol{k}, 1) = S_0(\boldsymbol{k})\alpha_1 + N(\boldsymbol{k}, 1) \tag{5}$$

Since the noise in different positions and times is mutually uncorrelated, we can describe $X_1(k)$ as:

$$X_1(k) = Y(\boldsymbol{k}, 1) + X_0(k)\alpha_1 \tag{6}$$

Similarly, when $n = 2$, $X_2(k)$ is defined as:

$$X_2(k) = Y(\boldsymbol{k}, 2) + X_1(k)\alpha_2 \tag{7}$$

Therefore, the enhanced frequency spectrum of stars in n can be represented as:

$$X_n(k) = Y(\boldsymbol{k}, n) + X_{n-1}(k)\alpha_n \tag{8}$$

To obtain the frequency spectrum of all the superposed frames, we can add the two-dimensional spatial Fourier transform of the current frame to the frequency spectrum of all the previous superposed frames, as shown in Equation (8). The result of the current frame will be superposed by the next frame, and this iteration can output the frequency spectrum of the enhanced stars of every frame easily.

In practical applications, digital images are represented by integer coordinates, and the velocity of stars needs to be converted to an integer to avoid artifacts. Let $I(x, y, f)$ be the input image with pixel coordinates x, y and frame number f. The image size is $M \times N$, and $x = 1, \ldots, M, y = 1, \ldots, N$. The two-dimensional spatial Fourier transform of the input image is given by:

$$FI(u, v, f) = \sum_{x=0}^{M-1} \sum_{y=0}^{N-1} I(x, y, f) e^{-i2\pi(\frac{ux}{M} + \frac{vy}{N})} \tag{9}$$

where (u, v) denotes the two-dimensional spatial wavenumber vector.

However, the velocity of stars in the f-th frame, denoted by $V_x(f)$ and $V_y(f)$, is typically non-integer. To address this, we introduce an offset of velocity ($D_{x-offset}(f)$ and $D_{y-offset}(f)$) to compensate for the error of converting velocity to an integer. This allows us to obtain a more accurate representation of the image without introducing artifacts. To determine the motion vector of the current frame ($D_x(f)$ and $D_y(f)$), we need to consider the offset of the velocity of the previous frame and the velocity of the current frame together. This ensures that the motion vector accurately reflects the movement of the stars in the image. The offset of the velocity of the previous frame and the velocity of the current frame is given as follows:

$$\begin{cases} D_x(f) = round\Big[V_x(f)t_0 + V_{x-offset}(f-1)t_0\Big] \\ D_y(f) = round\Big[V_y(f)t_0 + V_{y-offset}(f-1)t_0\Big] \end{cases} \tag{10}$$

$$\begin{cases} D_{x-offset}(f) = D_x(f) - V_x(f)t_0 \\ D_{y-offset}(f) = D_y(f) - V_y(f)t_0 \end{cases} \tag{11}$$

where $round(\cdot)$ means the process of rounding off. When f = 1, $V_{x-offset}$ and $V_{y-offset}$ are equal to 0. Now, we can deduce the phase matrix of motion spectrum as follows:

$$\alpha = exp\{-i(D_x u + vD_y)\} \tag{12}$$

Hence, according to Equations (9) and (12), Equation (8) can transform as:

$$FEI(u,v,f) = FI(u,v,f) + FEI(u,v,f-1) \cdot \alpha \tag{13}$$

Notably, the enhanced spectrum is equivalent to the original spectrum for the first frame component ($FEI(u,v,1) = FI(u,v,1)$). Furthermore, in actual observations, the visual field undergoes slow movement, with a maximum motion of two pixels per frame [47]. To optimize computing resources, a lookup table is introduced to determine the phase matrix of the motion spectrum, as shown in Figure 4. This approach allows for efficient processing as each iteration only requires the operation of Equations (9) and (13) and a single lookup.

$\alpha_{-2,2}$	$\alpha_{-1,2}$	$\alpha_{0,2}$	$\alpha_{1,2}$	$\alpha_{2,2}$
$\alpha_{-2,1}$	$\alpha_{-1,1}$	$\alpha_{0,1}$	$\alpha_{1,1}$	$\alpha_{2,1}$
$\alpha_{-2,0}$	$\alpha_{-1,0}$	$\alpha_{0,0}$	$\alpha_{1,0}$	$\alpha_{2,0}$
$\alpha_{-2,-1}$	$\alpha_{-1,-1}$	$\alpha_{0,-1}$	$\alpha_{1,-1}$	$\alpha_{2,-1}$
$\alpha_{-2,-2}$	$\alpha_{-1,-2}$	$\alpha_{0,-2}$	$\alpha_{1,-2}$	$\alpha_{2,-2}$

Figure 4. The lookup table of motion vector.

Furthermore, the stars that have just entered the field of view have fewer superposed frames than those almost leaving the field of view. Stars that have more superposed frames are enhanced to a greater degree. Therefore, to achieve adaptive threshold segments for different pixels, a mask of superposed frames is introduced. This mask helps to differentiate between pixels that have a high degree of superposition and those that do not, resulting in a more accurate representation of the image. The generation of this mask is similar to the star enhancement and can be described as follows:

$$FM(u,v,f) = E(u,v) + FM(u,v,f-1) \cdot \alpha \tag{14}$$

Here, $FM(u,v,f)$ is the spectrum of the mask of superposed frames, $E(u,v)$ denotes the two-dimensional spatial Fourier transform of the unit image, and alpha is a constant. In particular, $FM(u,v,1) = E(u,v)$. Figure 5 shows the generation of this mask. Owing to the invariability of the unit image of each frame, the procedure is easy to compute and implement.

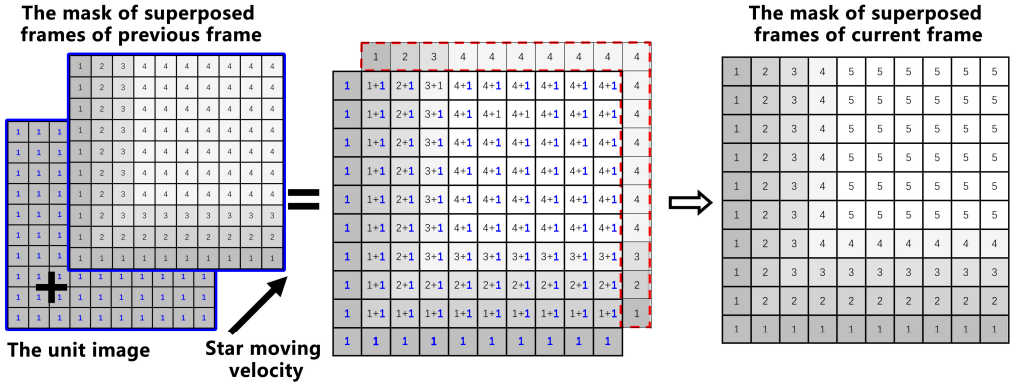

Figure 5. The implementation of the mask of superposed frames.

2.2. Adaptive Star Map

In order to improve the accuracy of star detection, an adaptive threshold segmentation approach is employed. This approach adjusts the threshold based on the number of superimposed frames for each pixel. Pixels with fewer superimposed frames are assigned a higher threshold to avoid false detection, while pixels with more superimposed frames are assigned a lower threshold to improve the detection rate. By using this approach, the algorithm can effectively detect stars while minimizing the impact of noise.

To determine the threshold for star detection, it is important to understand the probability distribution of stars, background, and noise. According to engineering practice, the noise in infrared images is distributed nearly normally [48]. Additionally, the temperature of deep space is less than 4 K [49], which has a negligible effect on stars. Therefore, in this paper, the background and noise are estimated using the normal distribution function. Suppose the distribution of background and noise is $\mathcal{N}(\mu_{noise}, {\sigma_{noise}}^2)$. Then, the stars can be expressed as $\mathcal{N}(\mu_{noise} + I_{star}, {\sigma_{noise}}^2)$, where μ_{noise} and σ_{noise} represent the mean and standard deviation of the noise, and I_{star} denotes the responsive intensity of the stars. Since the background noise is independent between different pixels and different frames, after n frames accumulation the distribution of the star and noise is still Gaussian, with the mean amplified by n times and the standard deviation amplified by $\sqrt{n}$ times. The noise and stars distribution will change to $\mathcal{N}(n\mu_{noise}, n{\sigma_{noise}}^2)$ and $\mathcal{N}(n\mu_{noise} + nI_{star}, n{\sigma_{noise}}^2)$, respectively. Ideally, the SNR of the stars will increase by a factor of $\sqrt{n}$. This superimposed process makes star detection easier, as shown in Figure 6.

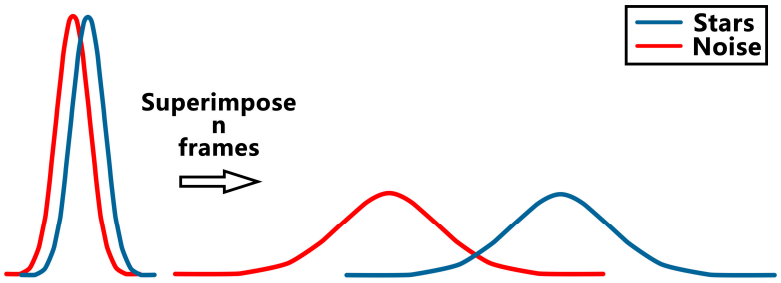

Figure 6. The probability distribution of stars and noise.

The calculation of the adaptive threshold is introduced in detail below. Firstly, the enhanced star image $EI(x, y, f)$ and the mask of superposed frames $M(x, y, f)$ is obtained by applying the inverse transformation of two-dimensional spatial Fourier as follows:

$$EI(x, y, f) = \frac{1}{MN} \sum_{u=0}^{U-1} \sum_{v=0}^{V-1} FEI(u, v, f) e^{i2\pi(\frac{ux}{M} + \frac{vy}{N})} \tag{15}$$

$$M(x, y, f) = \frac{1}{MN} \sum_{u=0}^{M-1} \sum_{v=0}^{N-1} FM(u, v, f) e^{i2\pi(\frac{ux}{M} + \frac{vy}{N})} \tag{16}$$

Then, we apply median filtering to eliminate stars and other targets. Once the background is relatively clean, we can estimate the mean (I_{mean}) and standard deviation (I_{std}) of the background. These values are used to calculate the threshold for eliminating noise and stars. We use the three sigma criteria along with an analysis of the probability distribution of stars and noise. By applying these criteria, we obtain the threshold for eliminating noise (T_{EN}) and the threshold for detecting stars (T_{DS}) as follows:

$$T_{EN}(x, y, f) = I_{mean}(f) \cdot M(x, y, f) + C_{\sigma N} \cdot I_{std}(f) \cdot \sqrt{M(x, y, f)} \tag{17}$$

$$T_{DS}(x, y, f) = [I_{mean}(f) + Psnr \cdot I_{std}(f)] M(x, y, f) + C_{\sigma S} \cdot I_{std}(f) \cdot \sqrt{M(x, y, f)} \tag{18}$$

where $Psnr$ denotes the lowest signal-to-noise ratio of the stars that plan to suppress. This parameter can limit the lower limit of the star SNR that needs to be suppressed and enhance the robustness of the proposed method for blurred images. Then, $C_{\sigma N}$ and $C_{\sigma S}$ are the coefficients of sigma for eliminating noise and the coefficients of sigma for detecting stars, respectively. The effectiveness of noise suppression in the image processing algorithm is directly proportional to the value of $C_{\sigma N}$. However, it is important to note that an excessively high value of $C_{\sigma N}$ may result in the erroneous detection of stars. Similarly, the selection of $C_{\sigma S}$ should aim to balance noise suppression and star detection. Typically, a value of $C_{\sigma N}$ greater than 4.5 and a value of $C_{\sigma S}$ greater than 3 are recommended. The specific parameter selection will be explained in Section 3.2. The optimal values of $C_{\sigma N}$ and $C_{\sigma S}$ can be increased with a higher $Psnr$. In practical applications, these parameters can be adjusted based on the acceptable level of false positives and missed detections. To obtain the final threshold (T_{star}), Equations (17) and (18) are used to calculate the number of frames that make T_{EN} and T_{DS} equal. The final threshold is obtained by fusing the two thresholds as in the below equation:

$$T_{star}(x,y,f) = \begin{cases} \frac{T_{EN}(x,y,f)+T_{DS}(x,y,f)}{2} & M(x,y,f) > \left(\frac{C_{\sigma 1}+C_{\sigma 2}}{Psnr}\right)^2 \\ T_{EN}(x,y,f) & M(x,y,f) \leq \left(\frac{C_{\sigma 1}+C_{\sigma 2}}{Psnr}\right)^2 \end{cases} \tag{19}$$

It is crucial to note that the selection of the final threshold depends on the number of available frames. Figure 7 depicts the probability distribution of star superposition with different frame numbers and the selection principle of the final threshold. In Figure 7a, the noise and the star have a lot of overlap, and it is not good to separate the two. Our primary objective is to eliminate noise and prevent false detection when the number of frames is less. Owing to the lack of enhanced frames, the stars are mixed with noise, thereby preventing false detection as the main object. Conversely, if we have sufficient frames, we have the conditions to distinguish the stars from the noise. Then, we will select the middle value of the threshold for eliminating noise and detecting stars as the final threshold, as shown in Figure 7b.

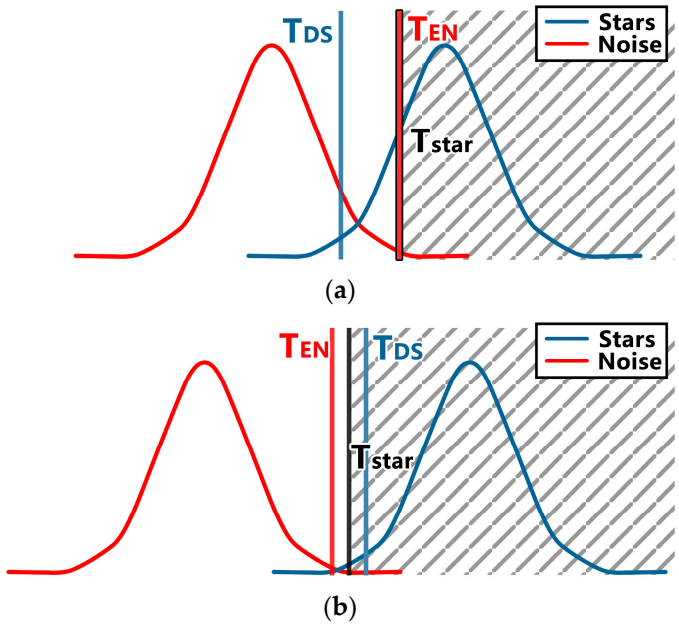

Figure 7. The selection principle of the final threshold: (**a**) noise elimination priority; (**b**) star detection and noise elimination are considered comprehensively.

After the above steps, the adaptive threshold is used to segment the mask of stars from the enhanced star image. The detection of stars can be suppressed to avoid their influence on the detection of other space objects. In some cases, it may be beneficial to further improve the suppression of the star background by applying a morphology dilation operation to the mask. This process should be chosen based on the specific optical system under consideration.

3. Experiment and Parameter Setting

In this section, we provide a detailed explanation of the experimental design. Meanwhile, the set value of the main parameters is discussed in order to obtain a good performance. Finally, the experimental results compared with other new methods are presented.

3.1. Experimental Setup

In this paper, three satellite real star data were used to verify the robustness and effectiveness of the proposed method. The parameters of the infrared camera used in this satellite are listed in Table 1.

Table 1. The parameters of infrared camera used in the satellite.

Parameters	Value
Format	512 × 512
The angle resolution of pixel	0.02464°
The angle of field of view	12.6° × 12.6°
Framerate	20 Hz
Bits per pixel	14 bits
Spectrum	2.1~3.3 μm
Field direction	Seq.1: De = 340.668 Ra = −46.885 Seq.2: De = 298.808 Ra = −59.196 Seq.3: De = 252.166 Ra = −69.028

To evaluate the effectiveness of the proposed method quantificationally in this paper, we made use of a star table obtained from NASA's Wide-field Infrared Survey Explorer (WISE) [50]. Figure 8 shows the procedure for simulating star images. Each color in the picture corresponds to a star. Arrows indicate camera acquisition direction. The main method was referenced from star identification described by Zhang Guangjun [51]. The simulation procedure involved the establishment of a celestial, satellite camera, and image coordinates. Next, rotation transformation and perspective projection transformation were employed to convert the stars in the star table to image coordinates. The response intensities of the stars in the resultant image were then calculated based on factors such as the minimum detectable star magnitude, corresponding SNR, as well as the star's magnitude in the star list. Subsequently, each star was simulated using the point diffusion function and its response intensity, as well as its sub-pixel position concerning the camera. It is worth noting that the point diffusion function was approximated by the circular symmetric two-dimensional Gaussian distribution. In addition to the aforementioned techniques, a nearly constant velocity model for camera motion was used following the method in [52]. A randomized approach was adopted to generate the initial right ascension and declination of the camera, as well as its initial moving speed within the range of 1~3 pixels/frame. Other simulation parameters, as well as their relevant values, are listed in Table 2. Overall, these simulation procedures accurately reflected the expected behavior of the proposed method in different scenarios, which validates the effectiveness of the proposed solution.

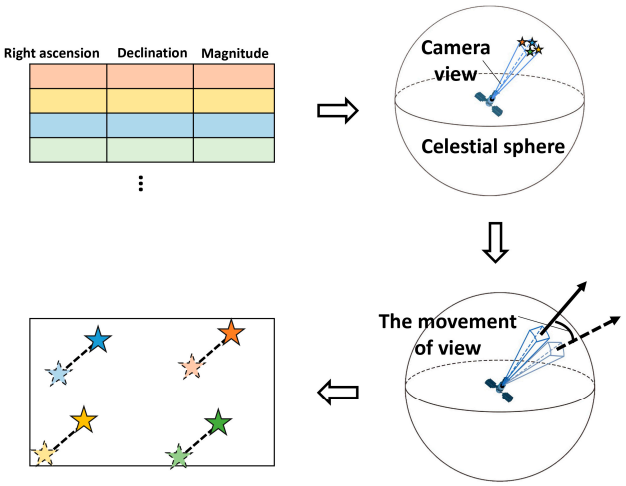

Figure 8. The procedure of simulating star images.

Table 2. The parameters of star map simulation.

Parameters	Value
Format	320 × 256
The angle resolution of pixel	0.01784°
The angle of field of view	4.568° × 5.710°
Framerate	30 Hz
Bits per pixel	14 bits
Spectrum	3 μm
Minimum detectable magnitude (corresponding SNR = 1)	9.56

To quantitatively analyze the effectiveness of the proposed method, three testing metrics are introduced: the accuracy of star suppression R_{ts}, the ratio of star suppression R_{ss}, and the average running time per frame T_{pf}. Suppose the number of stars suppressed by the method is N_s, and the number of stars correctly suppressed by the method is N_{true}. Furthermore, the number of stars whose SNR is larger than the lowest SNR of the stars that plan to suppress is N_{total}. Then, these metrics can be defined as follows:

$$R_{ts} = \frac{N_{true}}{N_s} \tag{20}$$

$$R_{ss} = \frac{N_{true}}{N_{total}} \tag{21}$$

3.2. Parameter Setting

To effectively suppress stars, it is crucial to determine the appropriate coefficients of sigma for both eliminating noise and detecting stars. To test the effectiveness of different coefficients, we conducted simulations and analyzed the results. Based on our findings, we will recommend the coefficients for optimal star suppression.

Where $N_{fsf}(n)$ refers to the frame amount that falsely suppressed the nth flickering pixel. As mentioned above, the evaluation of flickering pixel suppression uses simulation data. Therefore, the $N_{rf}(n)$, $N_{fsf}(n)$, and $N_{msf}(n)$ in Equations (13) and (14) can be recorded while the simulation is underway.

We introduce $R_{ts} \times R_{ss}$ to evaluate the performance of the proposed method. This index expresses the suppression precision and the suppressing rate, with a range of 0 to 1. A large value of $R_{ts} \times R_{ss}$ can only be obtained when the suppressed stars are many and

accurate. We simulate hundreds of star image sequences, each using different values of $C_{\sigma N}$, $C_{\sigma S}$, and SNR to suppress stars. The results of these tests are shown in Figures 9–11, with SNR values of 1, 1.5, and 2, respectively. Figures 9–11 (a) show the 3D map of $R_{ts} \times R_{ss}$ with different values of $C_{\sigma N}$ and $C_{\sigma S}$, while Figures 9–11 (b) show the distribution of $R_{ts} \times R_{ss}$ for different values of $C_{\sigma N}$ under maximum $C_{\sigma S}$, and Figures 9–11 (c) show the distribution of $R_{ts} \times R_{ss}$ for different values of $C_{\sigma S}$ under maximum $C_{\sigma N}$. It is clear that the suppression performance is better when $C_{\sigma N}$ is between 4 and 5 and when $C_{\sigma S}$ approaches 6. Table 3 provides a list of typical parameter selections.

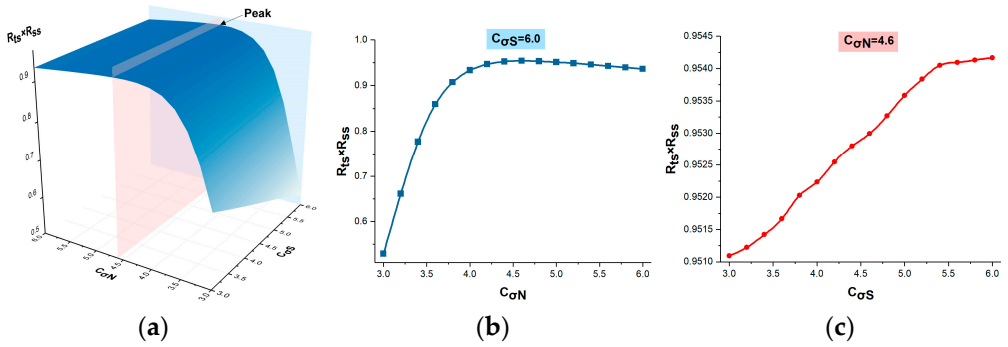

Figure 9. The distribution of $R_{ts} \times R_{ss}$ in Psnr = 1. (**a**) The 3D map of $R_{ts} \times R_{ss}$ with different values of $C_{\sigma N}$ and $C_{\sigma S}$; (**b**) the distribution of $R_{ts} \times R_{ss}$ for different values of $C_{\sigma N}$ under maximum $C_{\sigma S}$; (**c**) the distribution of $R_{ts} \times R_{ss}$ for different values of $C_{\sigma S}$ under maximum $C_{\sigma N}$.

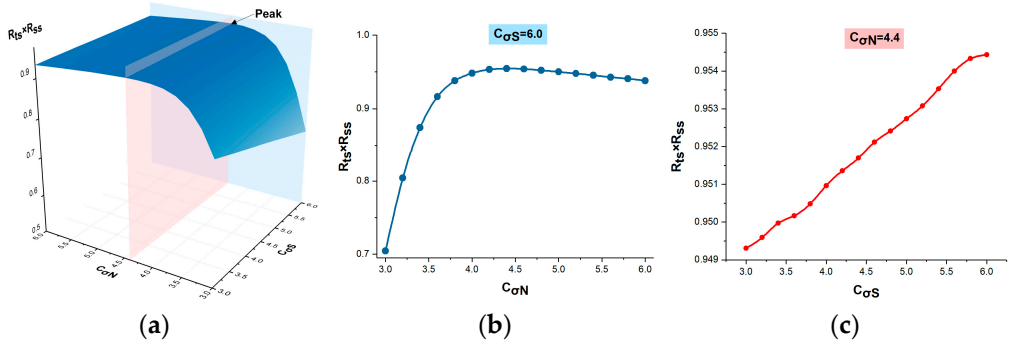

Figure 10. The distribution of $R_{ts} \times R_{ss}$ in Psnr = 1.5. (**a**) The 3-D map of $R_{ts} \times R_{ss}$ with different values of $C_{\sigma N}$ and $C_{\sigma S}$; (**b**) the distribution of $R_{ts} \times R_{ss}$ for different values of $C_{\sigma N}$ under maximum $C_{\sigma S}$; (**c**) the distribution of $R_{ts} \times R_{ss}$ for different values of $C_{\sigma S}$ under maximum $C_{\sigma N}$.

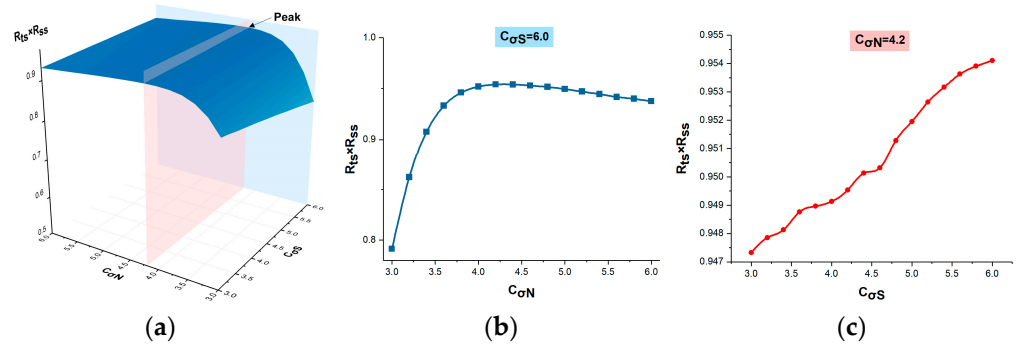

Figure 11. The distribution of $R_{ts} \times R_{ss}$ in Psnr = 2. (**a**) The 3-D map of $R_{ts} \times R_{ss}$ with different values of $C_{\sigma N}$ and $C_{\sigma S}$; (**b**) the distribution of $R_{ts} \times R_{ss}$ for different values of $C_{\sigma N}$ under maximum $C_{\sigma S}$; (**c**) the distribution of $R_{ts} \times R_{ss}$ for different values of $C_{\sigma S}$ under maximum $C_{\sigma N}$.

Table 3. The typical selection of parameters.

Psnr	$C_{\sigma N}$	$C_{\sigma S}$
1	4.2~4.8	5.5~6.0
1.5	4.0~4.6	5.6~6.0
2	4.0~4.4	5.8~6.0

3.3. Experimental Result

With the above experimental data and evaluation criterion, the proposed method is compared with star map registration via topology invariance (SMRTI) [26] and an enhanced moving target indicator (EMTI) [29]. The SMRTI and EMTI are the most recently proposed SBT and TBS, respectively. The proposed method uses the following parameter setting: $C_{\sigma N} = 4.6$, $C_{\sigma S} = 6$, $Psnr = 1$. The proposed method and other methods are implemented under MATLAB R2018a with an Intel Core 2.80 GHz processor and 8 GB of physical memory.

Figures 12–14 show the experimental results of real data Seq.1, Seq.2, and Seq.3, where (a), (b), and (c) are the result of the proposed method, SMRTI, and EMTI, respectively. The green star represents the real stars in the image. The red circle represents the stars suppressed by the proposed method in this paper. The blue box represents the stars suppressed by SMRTI, and the yellow triangle represents the stars suppressed by EMTI.

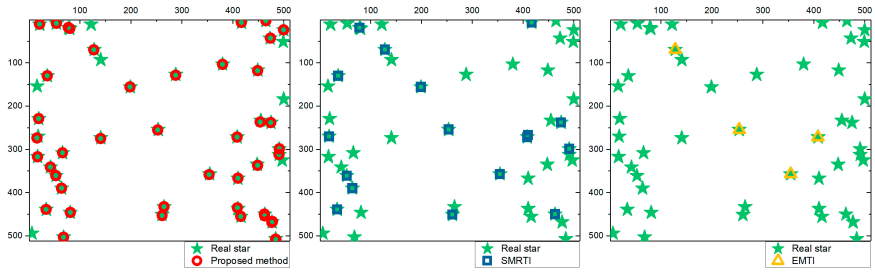

(**a**) (**b**) (**c**)

Figure 12. The experimental results with Seq.1 real data: (**a**) proposed method; (**b**) SMRTI; (**c**) EMTI.

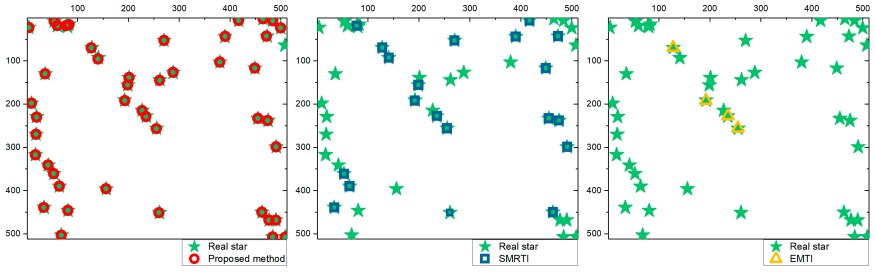

(**a**) (**b**) (**c**)

Figure 13. The experimental results with Seq.2 real data: (**a**) proposed method; (**b**) SMRTI; (**c**) EMTI.

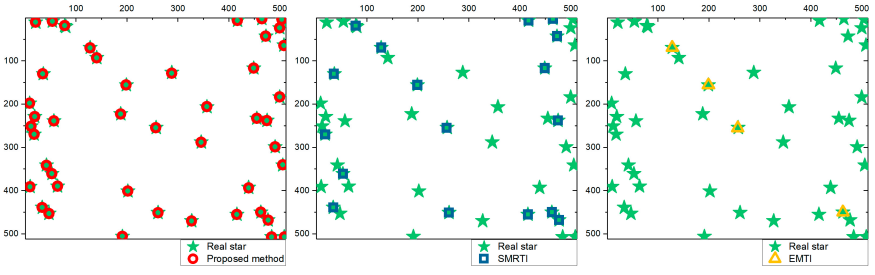

(**a**) (**b**) (**c**)

Figure 14. The experimental results with Seq.3 real data: (**a**) proposed method; (**b**) SMRTI; (**c**) EMTI.

Figure 15 presents the experimental results of the proposed method. In Figure 15a, the key frames of the simulated star image are shown, where most stars are obscured by noise. Figure 15b displays the enhanced star images using the proposed method, revealing many low-SNR stars that were previously hidden. Figure 15c shows the stars detected by the proposed method, with the blue block indicating the detected stars and the red stars representing the actual stars present in the images. While there were a few mistaken detections, the proposed method successfully identified most of the stars, with only a small quantity of stars being missed.

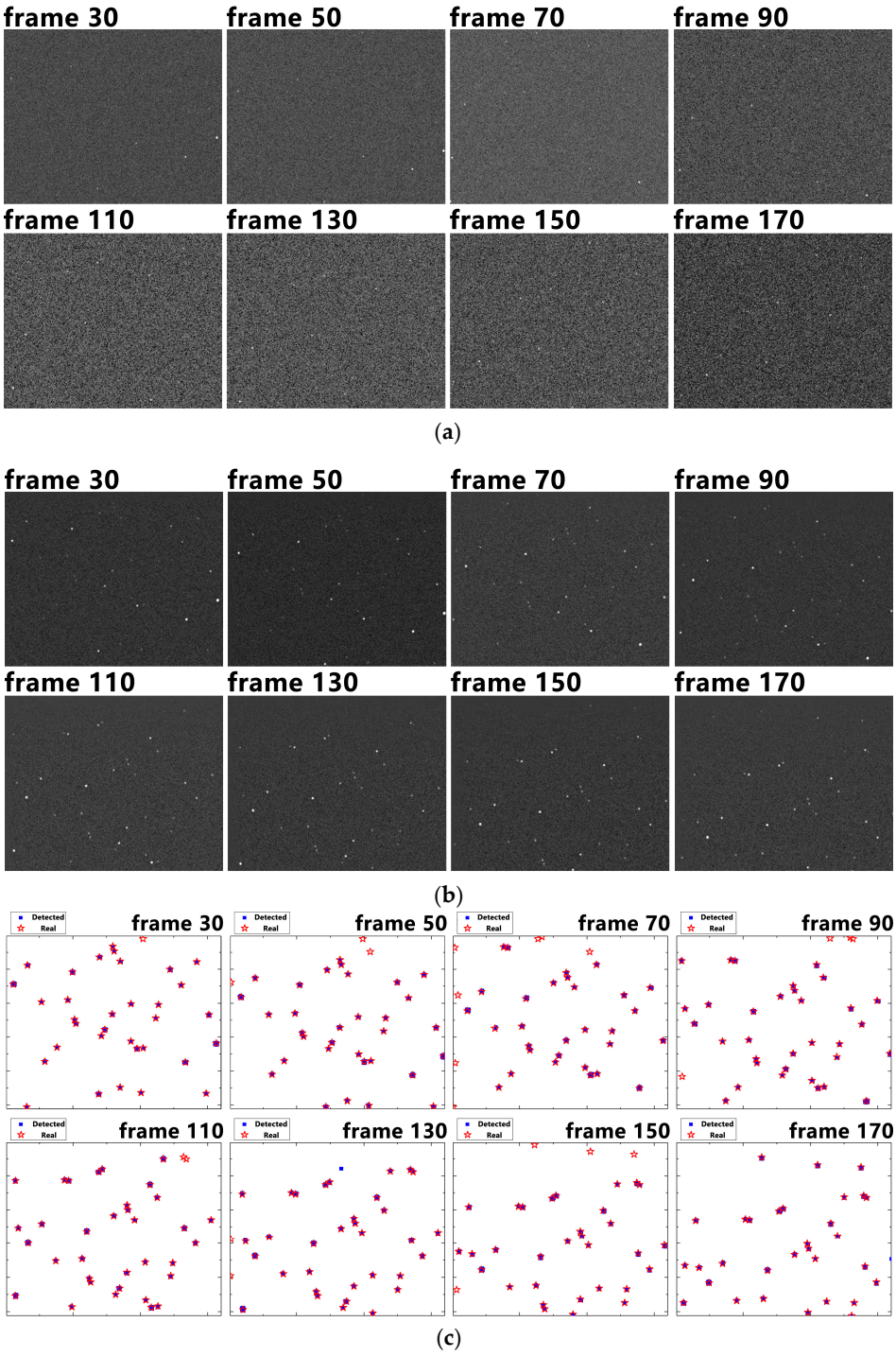

Figure 15. The experimental result of the proposed method. (**a**) Simulated star image sequence; (**b**) star image sequence enhanced advanced RMTI; (**c**) the stars detected by the proposed method.

We evaluated the performance of the three methods by recording the accuracy of star suppression (R_{ts}), the ratio of star suppression (R_{ss}), and the average running time per frame (T_{pf}) using a hundred simulation sequences. The results, presented in Table 4, demonstrate that the proposed method outperforms the other methods in terms of both speed and accuracy. Specifically, the proposed method achieves the task quickly and effectively, as evidenced by its high R_{ts} and low R_{ss} values.

Table 4. The experimental result of methods.

Method	R_{ts}	R_{ss}	T_{pf}
Proposed method	98.72%	98.82%	0.0031 s
SMRTI	98.19%	69.88%	0.2490 s
EMTI	98.59%	73.28%	0.0640 s

To offer a more intuitionistic star suppression result, the ratio of star suppression on a different SNR partition is recorded and mapped as follows.

4. Discussion

In the experiment with real data, the proposed method has an obvious advantage over other methods, as shown in Figures 12–14. The proposed method only misses a few stars. The effectiveness and robustness of the proposed method are demonstrated.

The working process shown in Figure 15 explains why the proposed method can suppress a dim star background. The proposed method for suppressing a dim star background is based on the core idea of treating stars as targets. By enhancing the SNR of stars through multi-frame accumulation, as shown in Figure 15b, the enhanced stars can be easily detected through threshold segmentation. Finally, the detected stars in Figure 15c are suppressed. The proposed method is capable of suppressing the majority of stars in the field of view, as seen in Figure 15c. However, a small minority of stars may be missed or wrongly suppressed in the top right corner of the subgraph of Figure 15c due to the lack of superimposed frames. If we do not accept the suppression results of this region, the accuracy of star suppression and the ratio of star suppression will be further improved. However, this comes at the expense of the field of view. Therefore, this promotion scheme should be considered according to the actual application situation. It is worth noting that the results compared with SMRTI and EMTI in Table 4 and Figure 16 are evaluated from the entire field of view.

Space target detection under a star background has been extensively researched, with a recent focus on high-SNR star suppression and corresponding DBT target detection methods. As shown in Table 4, the proposed star suppression method has a significant advantage in the ratio of star suppression. This advantage is mainly due to the effective suppression of low-SNR stars, as demonstrated in Figure 16. When the SNR is larger than five, these three methods are evenly matched. When the SNR ratio is smaller, the advantages of the proposed method are more obvious. The SMRTI and EMTI methods can suppress a few stars when the SNR is lower than two, and EMTI can suppress more stars than SMRTI when the SNR is between two and five. This is because EMTI adopts limited energy accumulation first. However, the proposed method enhances low-SNR stars through RMTI, resulting in stable and efficient star suppression when the SNR is lower than five. Although low-SNR stars do not interfere with SMRTI and EMTI, the proposed method's ability to suppress them is vital to TBD methods. This is the most significant contribution of our proposed method. The suppression of a low-SNR star background is an urgent issue, and the proposed method is on par with EMTI and SMRTI in terms of the accuracy of star suppression, with all three methods achieving over 98% accuracy. Additionally, the proposed method has a certain advantage in running time. These results demonstrate that the proposed method can be widely used in preprocessing for low-SNR target detection and tracking.

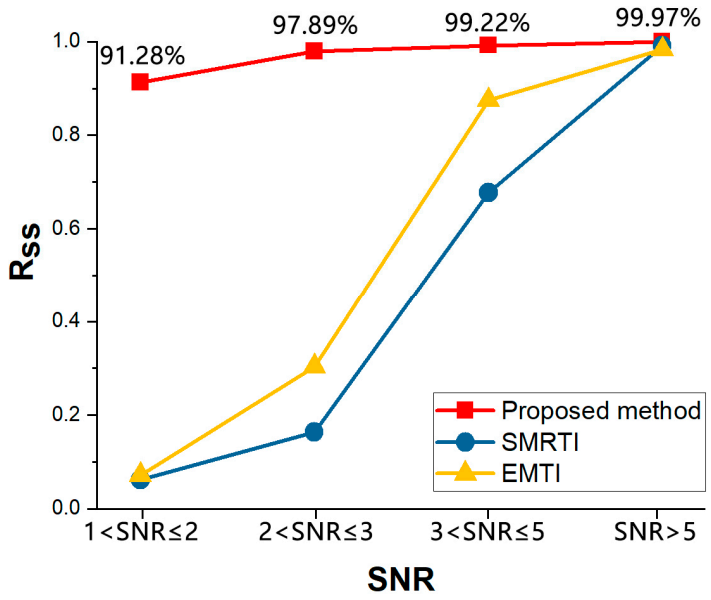

Figure 16. The ratio of star suppression on different SNR partitions.

5. Conclusions

To address the limitation of existing star suppression algorithms in effectively suppressing very-low-SNR star backgrounds, a dim star background suppression algorithm via RMTI is proposed in this paper. The proposed method involves enhancing the dim stars using advanced RMTI, followed by an adaptive threshold segmentation to filter out stars precisely. The experimental results using simulated star images demonstrate that the proposed method can stably and reliably suppress stars with an SNR of less than 2, with a star suppression rate of over 91%, and an overall star suppression accuracy of over 98.7%. Compared to the existing star suppression algorithms, the proposed method exhibits significant improvements in real-time performance and low-SNR star suppression ability. For real image processing, this method still maintains a good performance. As a preprocessing step for many TBD methods, the proposed method can effectively reduce the false detection rate of infrared dim small target detection and tracking and improve the real-time performance.

Author Contributions: All the authors contributed to this study. Conceptualization, L.Z. and P.R.; Investigation, L.Z. and Y.H.; Methodology, P.R. and X.C.; Resources, Y.H. and X.C.; Software, L.Z. and X.C.; Data curation, L.Z.; Funding acquisition, P.R. and L.J.; Project administration, Y.H. and X.C.; Supervision, L.J. Writing—Original draft preparation, L.Z. and P.R.; Writing—review and editing, P.R. and L.J.; Validation, L.J. All authors have read and agreed to the published version of the manuscript.

Funding: This research was funded by National Natural Science Foundation of China, grant number 62175251.

Data Availability Statement: Not applicable.

Conflicts of Interest: The authors declare no conflict of interest.

References

1. Wei, B.; Nener, B.D. Multi-Sensor Space Debris Tracking for Space Situational Awareness With Labeled Random Finite Sets. *IEEE Access* **2019**, *7*, 36991–37003. [CrossRef]
2. Xie, Z.; Chen, X.; Ren, Y.; Zhao, Y. Design and Analysis of Preload Control for Space Debris Impact Adhesion Capture Method. *IEEE Access* **2020**, *8*, 203845–203853. [CrossRef]
3. Guo, X.; Chen, T.; Liu, J.; Liu, Y.; An, Q. Dim Space Target Detection via Convolutional Neural Network in Single Optical Image. *IEEE Access* **2022**, *10*, 52306–52318. [CrossRef]
4. Liu, D.; Wang, X.; Xu, Z.; Li, Y.; Liu, W. Space target extraction and detection for wide-field surveillance. *Astron. Comput.* **2020**, *32*, 100408. [CrossRef]

5. Kwan, C.; Budavari, B. Enhancing small moving target detection performance in low-quality and long-range infrared videos using optical flow techniques. *Remote Sens.* **2020**, *12*, 4024. [CrossRef]
6. Rawat, S.S.; Verma, S.K.; Kumar, Y. Review on recent development in infrared small target detection algorithms. *Procedia Comput. Sci.* **2020**, *167*, 2496–2505. [CrossRef]
7. Zou, Y.; Zhao, J.; Wu, Y.; Wang, B.; Dong, L. Reverse Procedure Detection of Space Target Streaks Based on Motion Parameter Estimation. *IEEE Access* **2021**, *9*, 21823–21831. [CrossRef]
8. Zhao, F.; Wang, T.; Shao, S.; Zhang, E.; Lin, G. Infrared moving small-target detection via spatiotemporal consistency of trajectory points. *IEEE Geosci. Remote Sens. Lett.* **2020**, *17*, 122–126. [CrossRef]
9. Cao, Y.; Wang, G.; Yan, D.; Zhao, Z. Two Algorithms for the Detection and Tracking of Moving Vehicle Targets in Aerial Infrared Image Sequences. *Remote Sens.* **2016**, *8*, 28. [CrossRef]
10. Chen, S.T.; Jin, M.; Zhang, Y.Y.; Zhang, C. Infrared blind-pixel compensation algorithm based on generative adversarial networks and Poisson image blending. *Signal Image Video Process* **2020**, *14*, 77–85. [CrossRef]
11. Tchendjou, G.T.; Simeu, E. Detection, location and concealment of defective pixels in image sensors. *IEEE Trans. Emerg. Top. Comput.* **2021**, *9*, 664–679. [CrossRef]
12. Wan, M.; Ye, X.; Zhang, X.; Xu, Y.; Gu, G.; Chen, Q. Infrared small target tracking via gaussian curvature-based compressive convolution feature extraction. *IEEE Geosci. Remote Sens. Lett.* **2021**, *19*, 7000905. [CrossRef]
13. Wan, M.J.; Gu, G.H.; Cao, E.C.; Hu, X.B.; Qian, W.X.; Ren, K. In-frame and inter-frame information based infrared moving small target detection under complex cloud backgrounds. *Infrared Phys. Technol.* **2016**, *76*, 455–467. [CrossRef]
14. Li, M.; Peng, L.; Chen, Y.; Huang, S.; Qin, F.; Peng, Z. Mask Sparse Representation Based on Semantic Features for Thermal Infrared Target Tracking. *Remote Sens.* **2019**, *11*, 1967. [CrossRef]
15. Cao, L.; Wan, C.; Zhang, Y.; Li, N. Infrared radiation characteristic measure method of point target. *J. Infrared Millim. Waves* **2015**, *34*, 5. [CrossRef]
16. Jia, L.; Rao, P.; Chen, X.; Qiu, S. On-Board Flickering Pixel Dynamic Suppression Method Based on Multi-Feature Fusion. *Appl. Sci.* **2022**, *12*, 198. [CrossRef]
17. Zhou, D.; Wang, X. Stray Light Suppression of Wide-Field Surveillance in Complicated Situations. *IEEE Access* **2023**, *11*, 2424–2432. [CrossRef]
18. Xu, Z.; Liu, D.; Yan, C.; Hu, C. Stray light nonuniform background correction for a wide-field surveillance system. *Appl. Opt.* **2020**, *59*, 10719–10728. [CrossRef]
19. Johnson, C.R.; Sentovich, M.F.; Ho, C.q. Star Background Cancellation for Deep Space Surveillance. *IEEE Trans. Aerosp. Electron. Syst.* **1981**, *AES-17*, 314–319. [CrossRef]
20. Xue, D.; Sun, J.; Hu, Y.; Zheng, Y.; Zhu, Y.; Zhang, Y. Dim small target detection based on convolutinal neural network in star image. *Multimed. Tools Appl.* **2020**, *79*, 4681–4698. [CrossRef]
21. Jun, Z.; Hongjian, Z.; Dakai, S.; Li, W.; Yanpeng, W.; Chunyan, L. High sensitive automatic detection technique for space objects. *Infrared Laser Eng.* **2020**, *49*, 88–94.
22. Zhang, H.; Bai, Y.; Li, J. An algorithm of small and dim target detection in deep space background. In Proceedings of the 2009 International Conference on Information and Automation, Zhuhai, China, 22–24 June 2009; pp. 985–989.
23. Zhu, Y.; Hu, W.; Zhou, J.; Duan, F.; Sun, J.; Jiang, L. A new starry images matching method in dim and small space target detection. In Proceedings of the 2009 Fifth International Conference on Image and Graphics, Xi'an, China, 20–23 September 2009; pp. 447–450.
24. Luo, Q.; Gao, Z.; Xie, C. Improved GM-PHD filter based on threshold separation clusterer for space-based starry-sky background weak point target tracking. *Digit. Signal Process.* **2020**, *103*, 102766. [CrossRef]
25. Feng, L.; Xiaoliang, X.; Tongsheng, S. Space small targets detection based on maximum projection and quick registration. *Infrared Laser Eng.* **2016**, *45*, 145–150.
26. Jiang, F.; Yuan, J.; Qi, Y.; Liu, Z.; Cai, L. Space target detection based on the invariance of inter-satellite topology. In Proceedings of the 2022 IEEE 10th Joint International Information Technology and Artificial Intelligence Conference (ITAIC), Chongqing, China, 17–19 June 2022; pp. 2151–2155.
27. Hou, W.; Lei, Z.; Yu, Q.; Liu, X. Small target detection using main directional suppression high pass filter. *Optik* **2014**, *125*, 3017–3022. [CrossRef]
28. Jianlin, L.; Xijian, P.; Debao, M. A novel method of drift-scanning stars suppression based on the standardized linear filter. In Proceedings of the 2011 International Conference on Optical Instruments and Technology: Optoelectronic Imaging and Processing Technology, Beijing, China, 28 November 2011.
29. Zhang, Y.; Rao, P.; Jia, L.; Chen, X. Dim moving infrared target enhancement based on precise trajectory extraction. *Infrared Phys. Technol.* **2022**, *128*, 104374. [CrossRef]
30. Wenkang, D.; Zongxi, S. Detection and tracking of multi-space junks in star images. In Proceedings of the Eighth International Conference on Digital Image Processing (ICDIP 2016), Chengu, China, 20–22 May 2016; p. 100330N.
31. Dong, W.; Yan, W.; Zhao, L. Moving space target detection algorithm based on trajectory similarity. In Proceedings of the SPIE/COS Photonics Asia, Beijing, China, 11 October 2018; p. 108161B.

32. Chen, B.; Qin, S.; Dai, D. A Star Identification Algorithm based on Radial Basis Neural Network. In Proceedings of the 2022 4th International Academic Exchange Conference on Science and Technology Innovation (IAECST), Guangzhou, China, 9–11 December 2022; pp. 1274–1278.
33. Niu, Y.; Wei, X.; Li, J. Fast and Robust Star Identification Using Color Ratio Information. *IEEE Sens. J.* **2022**, *22*, 20401–20412. [CrossRef]
34. Mehta, D.S.; Chen, S.; Low, K.S. A Rotation-Invariant Additive Vector Sequence Based Star Pattern Recognition. *IEEE Trans. Aerosp. Electron. Syst.* **2019**, *55*, 689–705. [CrossRef]
35. Coupon, J.; Czakon, N.; Bosch, J.; Komiyama, Y.; Medezinski, E.; Miyazaki, S.; Oguri, M. The bright-star masks for the HSC-SSP survey. *Publ. Astron. Soc. Jpn.* **2018**, *70*, S7. [CrossRef]
36. Han, K.; Pei, H.; Huang, Z.; Huang, T.; Qin, S. Non-cooperative Space Target High-Speed Tracking Measuring Method Based on FPGA. In Proceedings of the 2022 7th International Conference on Image, Vision and Computing (ICIVC), Xi'an, China, 26–28 July 2022; pp. 222–231.
37. Li, Y.; Niu, Z.; Sun, Q.; Xiao, H. Background Suppression Method of Star Image Based on Improved CBDNet. In Proceedings of the 2022 3rd International Conference on Computer Vision, Image and Deep Learning & International Conference on Computer Engineering and Applications (CVIDL & ICCEA), Changchun, China, 20–22 May 2022; pp. 671–674.
38. Hu, Z.; Su, Y. Infrared target tracking based on improved particle filtering. *Int. J. Pattern Recognit. Artif. Intell.* **2021**, *35*, 2154015. [CrossRef]
39. Jia, L.; Rao, P.; Zhang, Y.; Su, Y.; Chen, X. Low-SNR Infrared Point Target Detection and Tracking via Saliency-Guided Double-Stage Particle Filter. *Sensors* **2022**, *22*, 2791. [CrossRef]
40. Barniv, Y. Dynamic Programming Solution for Detecting Dim Moving Targets. *IEEE Trans. Aerosp. Electron. Syst.* **1985**, *AES-21*, 144–156. [CrossRef]
41. Sun, X.; Liu, X.; Tang, Z.; Long, G.; Yu, Q. Real-time visual enhancement for infrared small dim targets in video. *Infrared Phys. Technol.* **2017**, *83*, 217–226. [CrossRef]
42. Liu, H.; Rosenfeld, A.; Bhattacharya, P. Hough-transform detection of lines in 3-D space. *Pattern Recognit. Lett.* **2000**, *21*, 843–849.
43. Kultanen, P.; Xu, L.; Oja, E. Randomized Hough transform (RHT). In Proceedings of the 10th International Conference on Pattern Recognition, Atlantic City, NJ, USA, 16–21 June 1990; Volume 631, pp. 631–635.
44. Reed, I.S.; Gagliardi, R.M.; Stotts, L.B. Optical moving target detection with 3-D matched filtering. *IEEE Trans. Aerosp. Electron. Syst.* **1988**, *24*, 327–336. [CrossRef]
45. Reed, I.S.; Gagliardi, R.M.; Stotts, L.B. A recursive moving-target-indication algorithm for optical image sequences. *IEEE Trans. Aerosp. Electron. Syst.* **1990**, *26*, 434–440. [CrossRef]
46. Hou, W.; Yu, Q.F.; Lei, Z.H.; Liu, X.C. A block-based improved recursive moving-target-indication algorithm. *Acta Phys. Sin.* **2014**, *63*, 13. [CrossRef]
47. Zongfu, H.; Jinzhen, W.; Zengping, C. Motion characteristics analysis of space target and stellar target in opto-electronic observation. *Opto-Electron. Eng.* **2012**, *39*, 67–72.
48. Ibarra-Castanedo, C.; González, D.; Klein, M.; Pilla, M.; Vallerand, S.; Maldague, X. Infrared image processing and data analysis. *Infrared Phys. Technol.* **2004**, *46*, 75–83. [CrossRef]
49. Hong, S.H.; Choi, G.B.; Baek, R.H.; Kang, H.S.; Jung, S.W.; Jeong, Y.H. Low-Temperature Performance of Nanoscale MOSFET for Deep-Space RF Applications. *IEEE Electron Device Lett.* **2008**, *29*, 775–777. [CrossRef]
50. Wright, E.L.; Eisenhardt, P.R.M.; Mainzer, A.K.; Ressler, M.E.; Cutri, R.M.; Jarrett, T.; Kirkpatrick, J.D.; Padgett, D.; McMillan, R.S.; Skrutskie, M.; et al. The Wide-field Infrared Survey Explorer (WISE): Mission Description and Initial On-orbit Performance. *Astron. J.* **2010**, *140*, 1868–1881. [CrossRef]
51. Zhang, G. *Star Identification*; Nation Defense Industry Press: Beijing, China, 2011.
52. Ristic, B.; Arulampalam, S.; Gordon, N. Detection and tracking of stealthy targets. In *Beyond the Kalman Filter Particle Filters for Tracking Applications*; Barton, D.K., Ed.; Artech House: Boston, MA, USA; London, UK, 2004; pp. 240–251.